EASR

Engineering and Applied Science Research

https://www.tci-thaijo.org/index.php/easr/index

Published by the Faculty of Engineering, Khon Kaen University, Thailand

Nanosized Fe_3O_4/SiO_2 core-shells fabricated from natural sands, magnetic properties, and their application for dye adsorption

Munasir*[1)], Ahmad Taufiq[2)], Ambarwati Teraningtyas[1)], Diah Hari Kusumawati[1)] and Zainul Arifin Imam Supardi[1)]

[1)]Physics Department, Faculty of Mathematics and Natural Science, Universitas Negeri Surabaya (Unesa), Jl. Ketintang, Surabaya, Indonesia
[2)]Physics Department, Faculty of Mathematics and Natural Science, Universitas Negeri Malang (UM), Jl. Surabaya, Malang, Indonesia

Received 21 February 2021
Revised 8 August 2021
Accepted 11 August 2021

Abstract

This work presents Fe_3O_4/SiO_2 core-shell fabrication. Silica (SiO_2) nanoparticles (NPs) were prepared from silica sand using a continuous method, and Fe_3O_4 NPs were prepared from iron sand using the co-precipitation route. For Fe_3O_4/SiO_2 core-shell fabrication, we used the wet mixing method, where the composition of Fe_3O_4 and SiO_2 NPs was varied, and polyethylene glycol (PEG) was used as a binder. With an in-situ technique, tetraethyl orthosilicate (TEOS) was used as the SiO_2 precursor to coat the surface of the Fe_3O_4 NPs and the mass ratio of SiO_2 and Fe_3O_4 NPs was modified by varying the composition of the TEOS. The samples were characterized as follows: the structure, functional groups, particle size, morphology, and the magnetic property of Fe_3O_4/SiO_2 was characterized via X-ray diffraction, energy dispersive X-ray, Fourier transform infrared, scanning electron microscopy, and vibrating sample magnetometer, respectively, and porosity analysis was conducted. The Fe_3O_4/SiO_2 composites were successfully synthesized using wet mixing and in situ methods. Specifically, the diffraction peaks show PEG ($2\theta \approx 19°$ and 23°) for samples prepared using the wet mixing technique. The presence of PEG in the Fe_3O_4/SiO_2 composites reduced the saturation magnetization of the Fe_3O_4 NPs significantly from 29.5 to 9.0 emu/g when synthesized using the wet mixing method, and from 29.5 to 19.8 emu/g when synthesized using in the situ method. Furthermore, the increasing SiO_2 NPs composition reduced the shell wall thickness significantly and enhanced the adsorption porosity of the Fe_3O_4/SiO_2 core-shells. The higher SiO_2 content led to a decrease in the porous volume of the Fe_3O_4/SiO_2 core-shells.

Keywords: Fe_3O_4/SiO_2, Magnetic nanoparticle, Dye color, Wastewater

1. Introduction

In domestic perspectives, such as agriculture, industry, and energy, clean water is an important issue and a problem for the environment [1]. Industrial development, urbanization, and high population growth can create limited availability of healthy water for consumption, which is now the world's top issue [1, 2]. The advanced technology of nanomaterials provides new hope for the possibility of efficiently removing pollutants and germs. This solution is used for detecting and eliminating chemicals, including metal contaminants (Cd, Cu, Ti, Ag, Ni, and Zn), other harmful chemicals (PO_4^{3-}, NH_3, NO_3^-, and NO_2^-), microbes, cyanide, organics, algae (e.g., cyanobacterial poisons), bacteria, viruses, parasites, and antibiotics from drinking water [3, 4]. Nanomaterials usually have higher active site densities per unit mass because of their larger specific surface area (SSA). Furthermore, nanomaterials exhibit better surface-free energy, thereby increasing surface reactivity.

Magnetite can absorb Cr (VI), Cu (II), Ni (II), and Pb (II) [5, 6] metals and can be used for adsorption of alkaloids [7], removal of heavy metals from wastewater [7, 8], and mitigation of toxins in wheat germ [9]. Previous researchers have promoted Fe_3O_4-based composite materials, such as Fe_3O_4/GO and Fe_3O_4/SiO_2, which are positive prospects as adsorbents for methylene-blue dye color [7, 10], neutral red, heavy metal, and poisons in water [2, 8, 11]. The Fe_3O_4/SiO_2 core-shell is a magnetic nanoparticle (MNP) that can be used as a chemo-sensor for Hg (II) in an aqueous solution [12]. Fe_3O_4 NPs and tetraethyl orthosilicate (TEOS) can be formed with single-core formation and various thicknesses in the shell using the microemulsion process. The core particle size and shell thickness influence the magnetic properties acting as a nucleus [13]. The superparamagnetic of Fe_3O_4/SiO_2 can also be synthesized using a standard deposition method, in which silica coats the surface of NP Fe_3O_4 using TEOS as a hydrolysis precursor. TEOS has certain advantages, including overcoming the Fe_3O_4 agglomeration behavior to maintain aggregation trends and the core in the core-shell system [14, 15]. Fe_3O_4/SiO_2 core-shells are a new material with excellent absorption performance that can be used for phosphate removal from water [16], Pb^{2+} ion removal from water solutions [17], removal of zinc from aqueous solutions [17], natural organic matter removal [15], magnetic resonance imaging, and drug delivery systems [18]. In addition, the Fe_3O_4/SiO_2 core-shell can be employed in biomedical fields [19, 20]. MNP synthesis has been performed using microemulsion [21], one-pot hydrothermal methods [21], and joint precipitation [22, 23]. MNP is an ex-situ method, which is wet mixing with media as a binder using polyethylene glycol [4]. In the in-situ technique, TEOS is used as a precursor and will act as a coating on the core surface of Fe_3O_4 nanoparticles (NPs)

*Corresponding author.
Email address: munasir_physics@unesa.ac.id
doi: 10.14456/easr.2022.35

[13]. An environmentally friendly or green synthesis method can also be employed to use plant extracts for a synthesis medium [23]. The fabrication methods have advantages and disadvantages. For example, the ex-situ method is the simplest and easiest, while the in-situ method can control the core size of the Fe_3O_4 NP and the thickness of the silica shell.

In this study, we synthesized a Fe_3O_4/SiO_2 nanocomposite using ex-situ and in situ methods. The nanocomposite was characterized, including the analysis of crystal structure, functional groups, magnetic properties, and the ability to absorb natural dyes such as methylene blue. In addition, the particle morphology was observed using the high magnification electron microscope to identify the core-shell structure of the Fe_3O_4/SiO_2 samples.

2. Materials and methods

2.1 Materials

The materials used in the synthesis of Fe_3O_4 and SiO_2 NPs and Fe_3O_4/SiO_2 core-shell were iron sand (98%), silica sand (99%), TEOS, polyethylene glycol (PEG), ethanol, and DI-water. We also employed pro-analysis chemicals, such as sodium hydroxide (NaOH), ammonium hydroxide (NH_4OH, 6.5 M), C_2H_5OH (ethanol), and (hydrochloride acid (HCl, Pro Analysis 37%), as the primary media in the synthesis process. The Fe_3O_4/SiO_2 core-shell was then prepared using ex-situ and in situ methods.

2.2 Synthesis methods

2.2.1 Preparation of Fe_3O_4 and SiO_2 nanoparticles

The preparation of Fe_3O_4 NPs from iron sand was performed using the co-precipitation method, and the preparation of NPs of SiO_2 from quartz sand was performed using the continuous method. The procedure for preparing and synthesizing powder Fe_3O_4 NPs using the co-precipitation method was described by Munasir et al. [4]. Sodium silicate was obtained directly from the extraction of quartz sand with an alkaline NaOH compound. Sodium silicate was in the form of a silica NP precursor [4, 21]. Furthermore, $Si(OH)_4$ slurry was prepared using the co-precipitation process [24-26]. The silicate-acid slurry was then washed with distilled water and dried in an oven to obtain SiO_2 NP powder.

The synthesis of Fe_3O_4 NPs used the co-precipitation method with iron sand (iron oxide, FeO content~30%-40%) as a raw material. The synthesis stage was as follows: (i) iron oxide was obtained by filtering it in an immersion process with HCl Pro Analysis (37%), while stirring for 20 h to obtain a yellow $FeCl_4$ solution; (ii) in the co-precipitation process, a base reaction was formed by adding NH_4OH in stages (titration) [4, 26-28], so that a solid black sediment was obtained (Figure 1(a)); (iii) the materials were washed with distilled water to pH 7 (neutral) (Figure 1(b)); and (iv) the filtration and drying process of the filtrate was performed in an oven. The complete synthesis process of the Fe_3O_4 NPs from iron sand was previously reported [4, 26, 27].

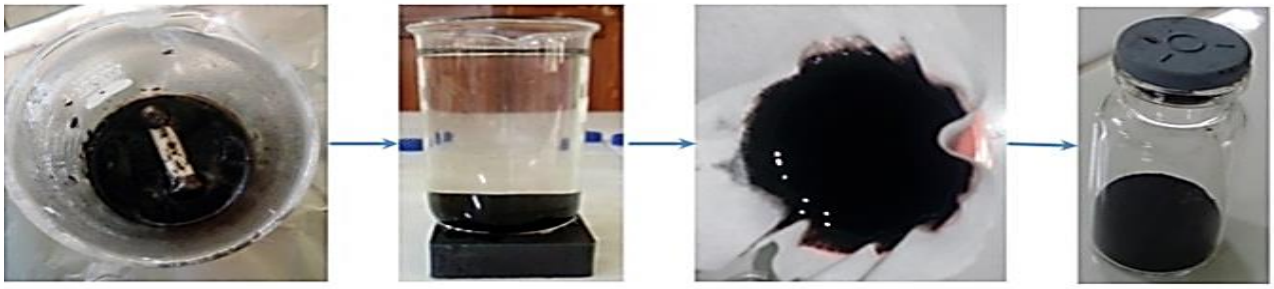

(a) (b) (c) (d)

Figure 1 Sequential synthesis of Fe_3O_4 NPs: (a) co-precipitation process, (b) washing process, (c) filtering process, and (d) the Fe_3O_4 NPs obtained from iron sand.

(a) (b) (c) (d) (e)

Figure 2 Continuous synthesis of SiO_2 NPs: (a) reaction of silica sand with HCl (*leaching process*), (b) reaction of quartz sand with NaOH (*sodium silicate-extraction*), (c) titration of the product (b) with the HCl solution, (d) filtration of product (c), and (e) SiO_2 NPs obtained from silica sand.

Silica (SiO_2) NPs were synthesized using a continuous method as follows: (i) the extraction of SiO_2 from quartz sand used HCl (2M (Figure 2(a)), (ii) the formation of the precursor sodium silicate (Na_2SiO_4) with the hydrothermal process used NaOH (6.5 M) (Figure 2(b)), (iii) the formation of silicide acid ($Si(OH)_4$) by co-precipitation used HCl (2M). The HCl was added gradually to the

precursor solution by titration until it reached pH~8-7 and a white silica slurry was formed (Figure 2(c)); (iv) the slurry was washed with distilled water to remove residue (NaCl); and (v) the solution was dried in a~100°C oven for 12 h to obtain a dry powder of SiO_2 NPs. In addition, the complete synthesis process of SiO_2 NPs from silica sand has been previously reported [6, 13, 19, 26].

2.2.2 Synthesis of Fe_3O_4/SiO_2 core-shell nanoparticles

(i). Wet mixing method: Fabrication of the Fe_3O_4/SiO_2 core-shell in this research follows two different methods. First is the ex situ method or wet mixing, which uses PEG 4000 as a binder to the substantial percentage approach (27,28). Second is the in situ method using TEOS with variations in volume composition [27]. This formation of the Fe_3O_4/SiO_2 composite used PEG as a binder [27, 29]. The variations in the mass ratio of Fe_3O_4 and SiO_2 are 1:1, 1:2, and 1:3, and PEG 4000 was the binder [4, 19, 26, 28-30].

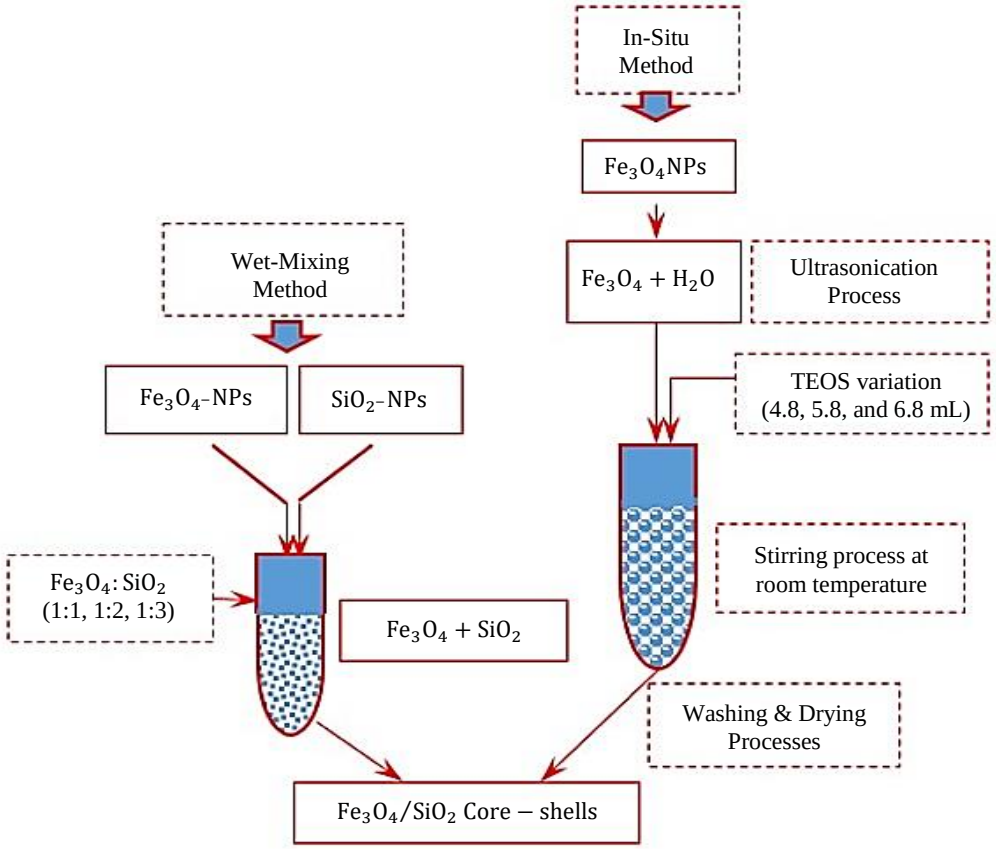

Figure 3 Schematic of the synthesis process for Fe_3O_4/SiO_2 core-shells.

The steps in the preparation of Fe_3O_4/SiO_2 using the wet mixing method are: (i) melting PEG 4000 powder (0.5 grams) at 60°C; (ii) preparing and adding Fe_3O_4 NP powder, while stirring until homogeneous; and (iii) adding SiO_2 NPs to the mixture of Fe_3O_4 and PEG 4000, while stirring until thoroughly mixed to obtain a nanocomposite. Samples with a composition of 1:1; 1:2; 1:3, and 3:1 were successfully prepared with mass ratios of Fe_3O_4 and SiO_2 NPs.

(ii). In situ method: The synthesis process of the Fe_3O_4/SiO_2 core-shell was conducted using the in-situ method as demonstrated in previous research by our team [27]. Briefly, the reaction of 1 gram of Fe_3O_4 NP powder and 24 mL distilled water was conducted by the ultra-sonication process for 30 min. Furthermore, 240 mL of ethanol was added to the mixture while stirring until it was interpreted as evenly mixed. Next, 4 mL of ammonia (6.5 M) and TEOS (with variations of 4.8, 5.8, and 6.8 mL) were added continuously (titration) and then stirred for 8 h at room temperature. The resulting brownish-black solution was washed with distilled water until a pH of 7; then the precipitation was filtered. The resulting precipitate was dried at 60°C for 24 h to form the Fe_3O_4/SiO_2 core-shell powders. For clarity, a schematic of the synthesis process for Fe_3O_4/SiO_2 core-shells can be seen in Figure 3.

2.3 Characterization of the Fe_3O_4/SiO_2 composite

The structural analysis and crystalline phase were analyzed using X-Ray diffraction (XRD) (Pan-Analytical, Type Expert-Pro). The microstructure or morphology analysis of samples was performed using scanning electron microscopy (SEM); the energy dispersive X-ray (EDX, FEI, Type: Inspect-S50) was used for the distribution (wt% or atomic at%) mapping of atomic elements from samples; the Fourier transform infrared (FTIR) [Type of equipment: Shimadzu 8400] was used to analyze the functional groups (molecules) in samples; transmission electron microscope (TEM) was used for core-shell microstructure analysis and to analyze particle size and the thickness of shell skin samples of Fe_3O_4/SiO_2. The Brunauer-Emmett-Teller (BET) instrument (Type of equipment: Quanta-chrome, Autosorb-1 series), with gas adsorption, principle nitrogen in prior samples (granules: nanosized particles) was used to calculate the SSA, diameter pore, and volume pore. The properties of the magnetic hysteresis loops were recorded using the vibrating sample magnetometer (VSM) (7404, Lakeshore, USA) at room temperature. A magnetization test was conducted on samples of Fe_3O_4 and Fe_3O_4/SiO_2 (powders) to determine the magnetic susceptibility of the material and its hysteresis curve.

3. Results and discussion

3.1 Structural analysis of Fe_3O_4/SiO_2 core-shell nanoparticles

Magnetite contains Fe (II) and Fe (III) oxides, and its crystalline structure is in the form of an inverted spinel, where the octahedral (Oh) holes are occupied by Fe (II) and Fe (III), and the tetrahedral (Td) holes are occupied by Fe (III). Fe (III) ions are equally divided between Oh and Td, both of which are anti-ferromagnetic and, therefore, do not contribute to the magnetic moment [31, 32]. The first characterization was conducted to determine the crystalline structure and phases of Fe_3O_4 and SiO_2 in Fe_3O_4/SO_2 composite samples, respectively, for 1:1, 1:2, and 1:3 ratios of Fe_3O_4:SiO_2 (prepared by wet mixing method) and 4.8, 5.8, and 6.8 mL TEOS (prepared by an in-situ method). The XRD test results present the characteristic peaks corresponding to the crystallographic planes (220), (311), (440), (422), and (511) of a crystalline structure of Fe_3O_4 (Figure 4(b-h)) (refer to the pdf reference database No. 01-088-0866) and the broad diffraction pattern at positions 2θ≈18°-32° of a non-crystalline (amorphous) structure of the SiO_2 phase (Figure 4(a)) [21, 27, 33].

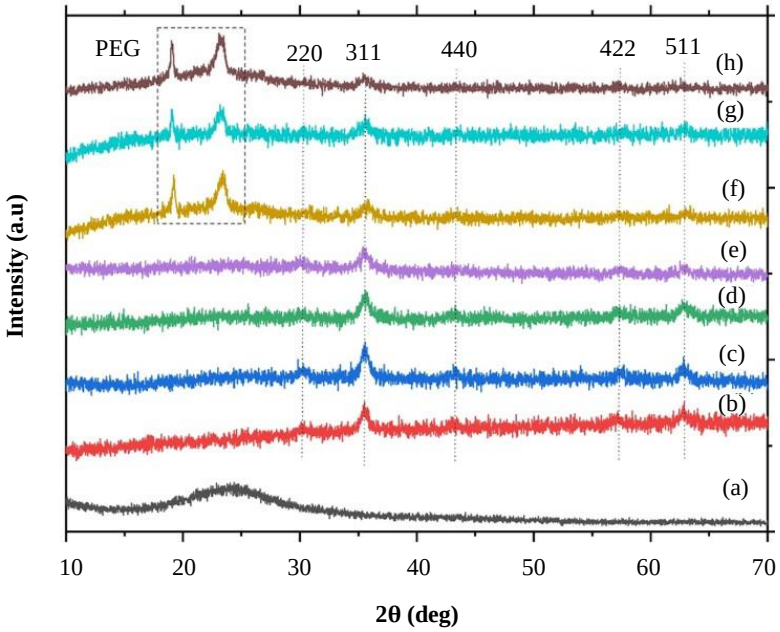

Figure 4 XRD Patterns of (a) SiO_2, (b) Fe_3O_4, (c-e) Fe_3O_4/SiO_2 synthesized using in situ method with various mass ratios of Fe_3O_4:SiO_2 (1:1, 1:2, and 1:3), and (f-h) Fe_3O_4/SiO_2 synthesized using wet mixing method with various TEOS volume (4.8, 5.8, and 6.8 mL).

The characterization of Fe_3O_4/SO_2 core-shell observed using XRD was used to confirm the new structure of the two combined materials, namely Fe_3O_4 and SiO_2. Figure 4(f-h) shows the results of the XRD diffraction patterns of Fe_3O_4/SiO_2 NP with composition variations that were prepared using the wet mixing method. The diffraction patterns of Fe_3O_4 and SiO_2 accompany the PEG diffraction peaks at 2θ≈19° and 23°. The existence of these two diffraction peaks has been identified as a PEG diffraction pattern [4, 13]. From the diffraction patterns, we understood that the Fe_3O_4/SiO_2 composites were successfully formed. The diffraction pattern on Fe_3O_4/SiO_3 NPs (Figure 4(c-e)) was the same as that shown by Fe_3O_4 NPs (Figure 4(b)). However, the crystalline phase of Fe_3O_4 NPs and Fe_3O_4/SO_2 nanocomposites prepared using the wet mixing and in situ methods still produced weak diffraction peaks [4, 25, 30, 34, 35].

3.2 Functional group analysis of Fe_3O_4/SiO_2 core-shells

FTIR is used to determine the absorption patterns of the functional groups of atoms forming materials. The FTIR test results of Fe_3O_4, SiO_2, and Fe_3O_4/SO_2 nanocomposite show the relationship between the wavenumbers and transmittance; the results of the analysis are presented in Figure 5 and Table 1. The pattern of absorption of the Fe_3O_4/SO_2 nanocomposite is presented in Table 1; the confirmation and matching of functional groups were conducted with the assistance of the results of previous studies. The infrared absorption range of 400-4000 cm^{-1} was considered to study the characteristics of the functional groups in SiO_2 and ferromagnetic Fe_3O_4 in the core-shell samples. Based on previous studies, the infrared absorption of the Si-O bond rocking vibration ranges from 465 to 475 cm^{-1} [25, 34].

The results of FTIR characterization in this study were similar to the previous studies; there were shaking vibrations of the Si-O bond at 468 cm^{-1} and the O-H (silanol) bond in the wavenumber range of 800-870 cm^{-1}, which is a characteristic of the SiO_2 molecule [4, 34, 35]. In addition, for the O-H bond water molecule, the absorption peak was in the wavenumber range of 1050-1115 cm^{-1} [4, 28]. At the wavenumber of 1649 cm^{-1}, there is an asymmetric Si-O-Si vibration, and at a wavelength of 3.517 cm^{-1}, the O-H bonds of silanol and water molecules were observed. Furthermore, Fe-O-Fe group vibrations were in the wavenumber range of 572-587 cm^{-1}, which indicated the presence of Fe_3O_4 in the Fe_3O_4/SiO_2 core-shell. Symmetrical stretching vibrations of Si-O-Si and Si-O bonds occurred in the range of wavenumbers of 793, 1092-1098 cm, and 954-964 cm^{-1} [25]. The core-shell prepared using the wet mixing method showed the C-O bond vibrations at 1342 and 1635 cm^{-1} that were caused by the influence of the PEG media binder. The functional group for the H-C-H bond was at 1351 and 1637 cm^{-1} [28, 33, 34]. Referring to the C_2H bond vibration, a CH (water molecule) may also occur at 2919 and 3313 cm^{-1} [33]. As shown in Figure 5, the vibration of the functional group occurs at 2923 and 3453 cm^{-1}. The vibration of the O-H functional group occurred at 3313 cm^{-1} [23, 29].

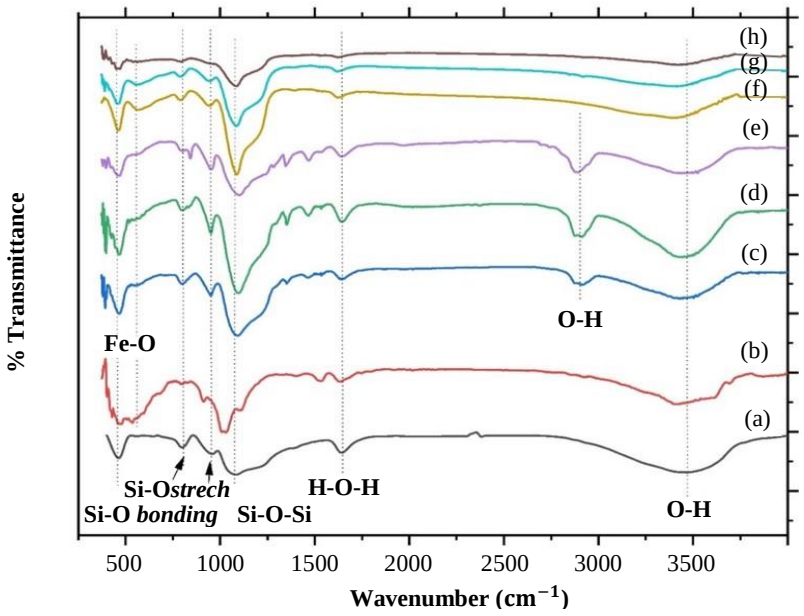

Figure 5 The infrared spectra of (a) SiO_2, (b) Fe_3O_4, (c-e) Fe_3O_4/SiO_2 nanocomposites synthesized using the in-situ method with various mass ratios of Fe_3O_4:SiO_2 (1:1, 1:2, and 1:3), and (f-h) Fe_3O_4/SiO_2 synthesized using the wet mixing method with TEOS volumes of 4.8, 5.8, and 6.8 mL

Table 1 The functional groups of Fe_3O_4, SiO_2 NPs, and Fe_3O_4/SiO_2 nanocomposites, prepared using wet mixing and in situ methods.

Wave numbers (cm^{-1})		Functional groups	References
Fe_3O_4/SiO_2	Ref.		
465	465-475	Si-O bond rocking	[4]
586	572-587	Functional group vibration of Fe-O-Fe	[25]
791	793	Si-O-Si symmetric stretching	[34]
951	954-964	Si-O symmetric stretching	[24, 34]
1091	1061-1098	Si-O-Si stretching	[25]
1351	1342	C-O bending	[34]
1637	1635	Bonding vibration of H-C-H	[34]
2919	2923	Bonding vibration of C-H	[33, 35]
3313	3000-3800	Functional group vibration of O-H	[23, 24, 29, 33]

3.3 Morphology of Fe_3O_4/SiO_2 core-shells nanoparticles

Figure 6 shows the morphology of the sample Fe_3O_4/SiO_2 prepared using ex situ (wet mixing) and in situ methods. The surface of the samples comprised Fe_3O_4 and SiO_2: (a) 1:3 (Sample #3, ex-situ) and (b) 6.8 ml TEOS (Sample #3, in-situ). Fe_3O_4/SiO_2 particles form more regular agglomeration with large particle sizes and more homogeneous spherical forms, with dominating formations such as silica SiO_2 particles (28). Most SiO_2 in the form of spheroids and Fe_3O_4 NPs tend to nonuniform distribution. Based on these two samples depicting particle formations (Figures 6(a) and 6(b)), the particle size and shape were nearly the same. However, the particle size is shown in Figure 6(b) tended to be larger and denser. This is thought to have an effect on sample characteristics, such as porosity and adsorption ability. The particle is nanosized (size<100 nm) (28).

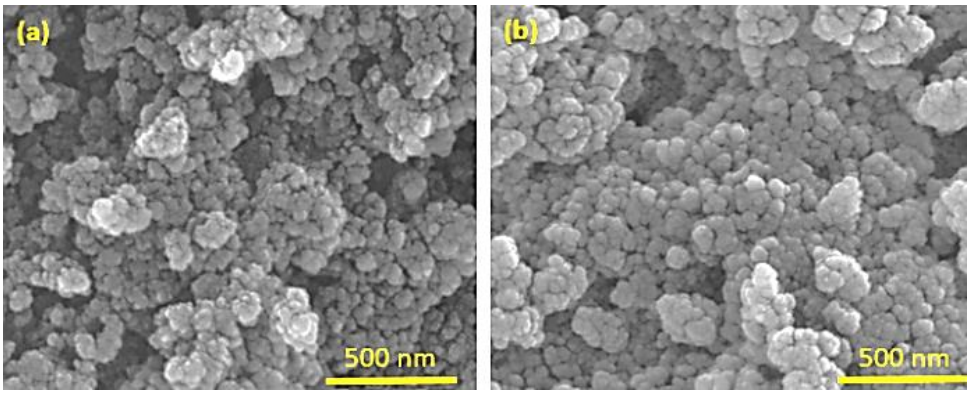

Figure 6 SEM Images of the Fe_3O_4/SiO_2 core-shells synthesized using (a) the wet mixing (#1:3) and (b) in situ (#6.8 mL) methods.

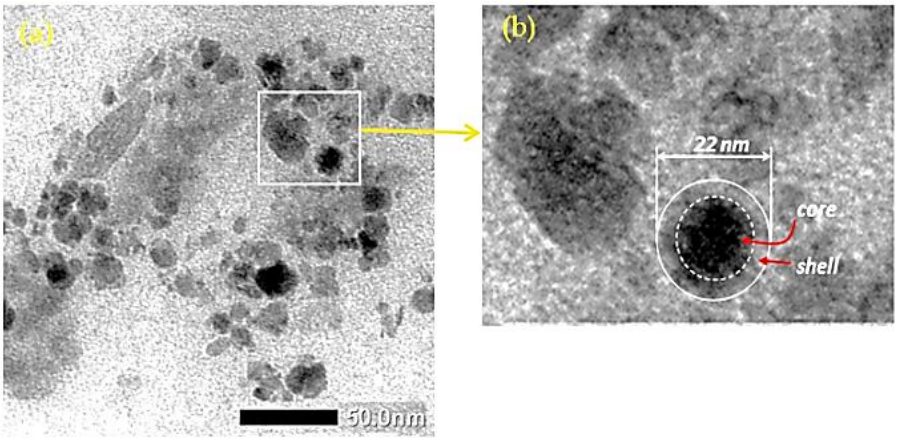

Figure 7 TEM Images of Fe_3O_4/SiO_2 core-shells synthesized using the wet mixing method (#1:3): (a) image with a scale of 50 nm. (b) Magnification of (a) showing the core-shell formation, with an estimated outer diameter of 22 nm.

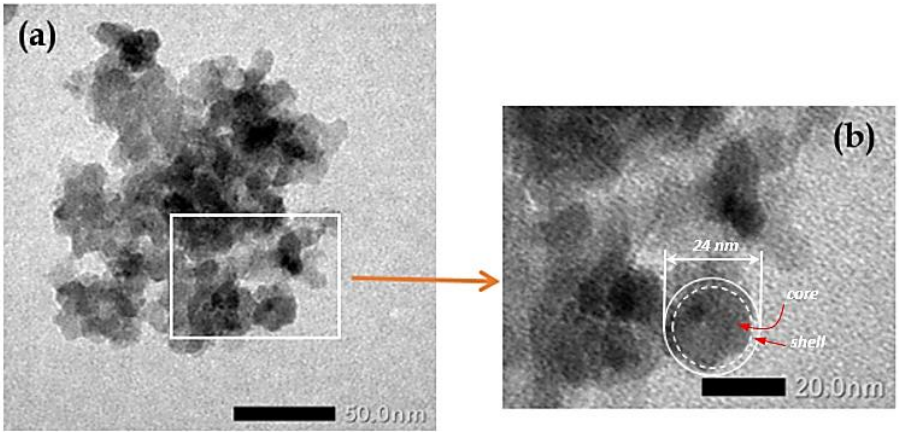

Figure 8 TEM Images of Fe_3O_4/SiO_2 core-shells synthesized using the in-situ method (#6.8 mL): (a) image with a scale of 50 nm. (b) Magnification of (a) showing the core-shell formation, with an estimated outer diameter of 24 nm.

As shown in Figures 7 and 8, we can observe the results of the microstructure characterization of the samples of Fe_3O_4/SiO_2 using the TEM, which shows the shape of a found core-shell formation. Figure 7 is an example of the microstructure of the Fe_3O_4/SiO_2 nanocomposite prepared using the wet mixing method, with a magnification scale of 50 nm (Figure 7(a)). If magnified, a shell-shell pattern is observed as shown in Figure 7(b); the darker colors (center position) are confirmed as Fe_3O_4 NPs (as the nucleus) and the brighter ring-like pattern on the outside is SiO_2 NPs (as a shell). The results of this microstructure observation also provide evidence that this type of shell-core formation is single core (15,19,23). The morphological formation of Fe_3O_4/SiO_2 prepared using the in-situ method is shown in Figure 8. The results of the microstructure analysis also showed that nucleation and shell formation had occurred. The homogeneity of the distribution of SiO_2 and Fe_3O_4 NPs in the core-shell synthesis can be more conditioned using the in-situ method [21]. The particle size of Fe_3O_4/SiO_2 is~68 nm, with the core size being~26 nm and the shell thickness being~17 nm, as observed in Figures 7 and 8. This is in line with previous research. The Fe_3O_4 and SiO_2 particles formed a shell-core system, in which Fe_3O_4 particles formed the nucleus and SiO_2 particles were the shells. The Fe_3O_4/SiO_2 particles are round with a diameter of~40-75 nm. Agglomeration occurs between SiO_2 particles, with a core size of 35 nm and a shell thickness 20 nm [6].

4. Magnetic properties of Fe_3O_4/SiO_2 core-shells nanoparticles

4.1 Preparation using wet mixing method

The magnetic properties of the Fe_3O_4/SiO_2 samples were characterized using a VSM (device type 7404, Lakeshore, USA). In this method, the powder particles of SiO_2 were mixed with Fe_3O_4 and PEG media. The results were saturation-hysteresis and magnetization curves, as shown in Figure 9. The samples prepared with Fe_3O_4 NP powder were included in TEOS. The butanol solution was then distorted to obtain the Fe_3O_4/SiO_2 deposits; this process is the tendency of the in-situ method, and the results of the hysteresis curve are shown in Figures 9(b-d). In general, the types of curves of the two sample groups soft magnetic and superparamagnetic are the same with different magnetization values (M) for different magnetic strengths (Hc). They do not show saturation at 22,000 Oe for magnetic fields.

As shown in Figure 9, samples of the Fe_3O_4 prepared using the wet mixing method showed decreased magnetization rates for increasing SiO_2 particle composition (Figures 9(b-d)); the magnetization value decreased significantly compared with the Fe_3O_4 sample (Figures 9(a)). The increased composition of SiO_2 has implications for shell thickening in core-shell systems such as morphological photographs (Figure 8(b)) (6,15). When compared with the Fe_3O_4 sample, the magnetization of Fe_3O_4/SiO_2 experienced a weakening from ~29.5 to 9 emu/g (Sample #1, Figure 9(b)), which resulted in a decrease of up to 20 emu/g (67.8%); to 7 emu/g (Sample #2, Figure 9(c)), reduced to 22 emu/g (74.6%), and to 5 emu/g (Sample #3, Figure 9(d)), reduced to 24 emu/g (81.4%).

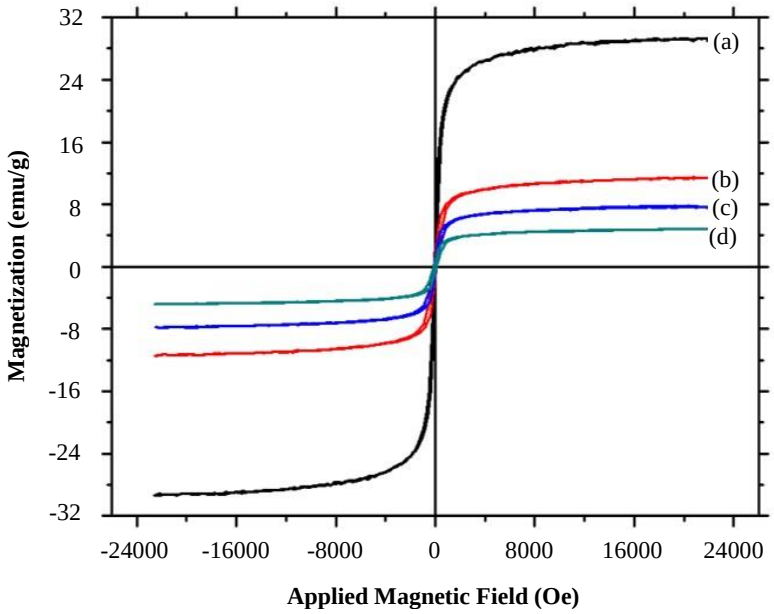

Figure 9 Hysteresis curves of (a) Fe_3O_4-NPs and Fe_3O_4/SiO_2 core-shells synthesized using wet the mixing method with a mass ratio of Fe_3O_4:SiO_2 (b) (1:1), (c) (1:2), and (d) (1:3).

4.2 Prepared using in-situ method

According to theoretical studies, the wider the hysteresis loop, the greater the magnetic susceptibility, and vice versa. Furthermore, the width or narrowness of the hysteresis loop will also indicate the type of soft or hard magnetic materials [35]; (a) hard magnets (hard magnetic) and (b) soft magnets (soft magnetic) have different characteristics. Hard magnets can maintain their magnetic properties when an external magnetic field is introduced or after the process is magnetized. Soft magnets (soft magnetic) are easy to magnetize and can easily lose their magnetism if they are not constantly magnetized [9]. As shown in Figure 10, the results of the measurements of the magnetic hysteresis of the sample Fe_3O_4/SiO_2 core-shell prepared using the in-situ method exhibit decreasing magnetization with the addition of layers of SiO_2 particle as a wrapper for Fe_3O_4 particles. The magnitude of magnetization decreased from~29.5 to 19.8 emu/g, along with an increase in the volume of TEOS (4.8, 5.8, and 6.8 ml) for samples prepared using the in-situ method (see Figures 10(b-d)). When compared with the Fe_3O_4 sample, magnetization of Fe_3O_4/SiO_2 experienced a weakening trend from~29.5 to 19.8 emu/g (TEOS 4.8 ml, Figure 10(b)), which resulted in a decrease of up to 9.7 emu/g (32.9%); to 18.5 emu/g (TEOS 5.8 ml, Figure 10(c)), reduced to 11 emu/g (37.3%), and 16.9 emu/g (TEOS 6.8 ml, Figure 10(d)), reduced to 12.6 emu/g (42.7%).

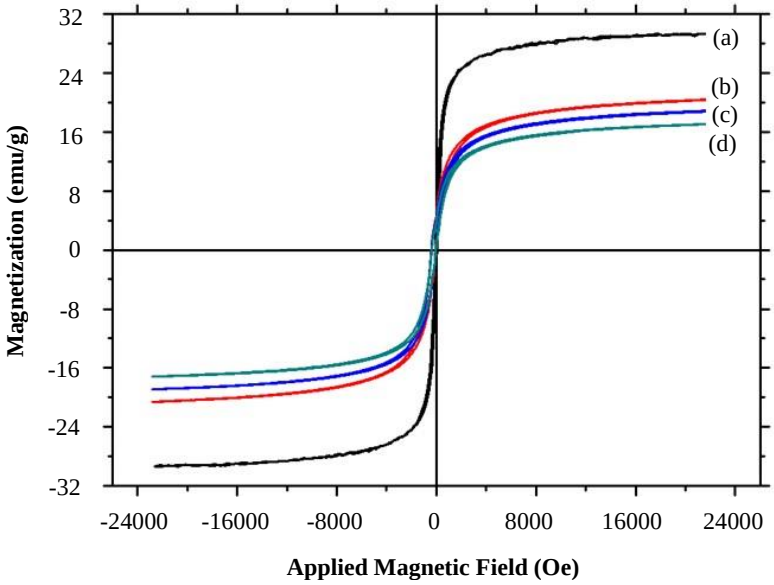

Figure 10 Hysteresis curves of (a) Fe_3O_4-NPs and Fe_3O_4/SiO_2 core-shells synthesized using in situ methods with a TEOS volume of (b) 4.8, (c) 5.8, and (d) 6.8 mL

Comparison of the magnetic properties of the samples of the Fe_3O_4/SiO_2 prepared using the wet mixing and in situ methods are presented in Figure 11. For the samples prepared using the wet mixing method, the magnetization value was lower than those of the samples prepared using the in-situ method (Figures 11(b) and 11(c)). However, the pattern and shape of the curve are nearly the same. Quantitatively, the area of the Fe_3O_4/SiO_2 core-shell hysteresis curve prepared using the in-situ method appears wider. Therefore, qualitatively and quantitatively, they strengthen each other [21, 33].

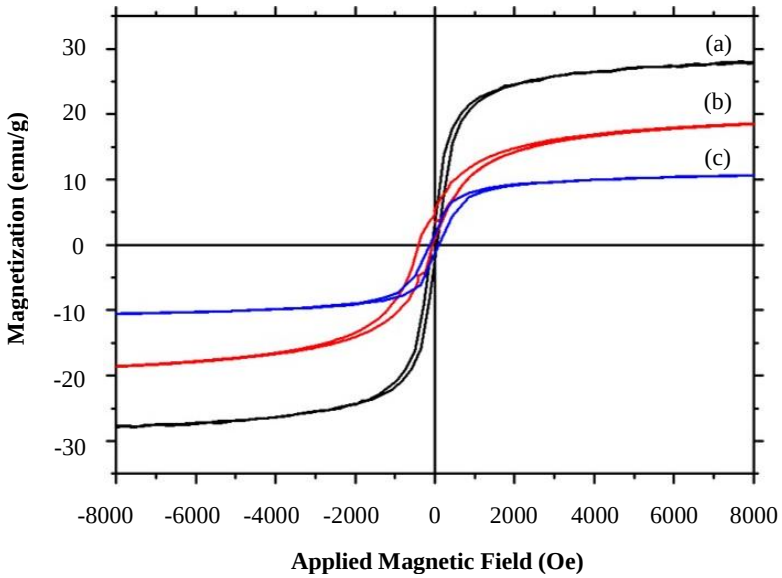

Figure 11 Hysteresis curves of (a) Fe_3O_4-NPs and Fe_3O_4/SiO_2 core-shells synthesized using (b) wet mixing and (c) in situ methods.

4.3 Porosity of the Fe_3O_4/SiO_2 core-shells nanoparticles

BET is a method used to characterize the surface area, pore diameter, and volume of a material. Figure 12 shows the P/P_0 curve to the pore volume, the adsorption and desorption of the Fe_3O_4/SiO_2 samples, and the BET test results data (Quanta-chrome device type, Autosorb-1 Series), using nitrogen gas (vapor point, 77K). The data was then analyzed by the BET and BJH methods. The 1:2 sample had the largest surface area and volume. The value then decreases for 1:3, and the smallest was the 3:1 sample. Changes in the variations of mass composition of Fe_3O_4 and SiO_2 affect the surface area and volume of Fe_3O_4/SiO_2. Figure 12 shows the volume distribution of pore volume during the adsorption and desorption of nitrogen gas on Fe_3O_4/SiO_2 particles. An increase in SiO_2 composition or shell thickness increased the volume of the porous samples for the 1:2 and 1:3 compositions compared with the increase in the composition of SiO_2 NPs (1:3 sample). Therefore, the presence of SiO_2 as a coating material on porous Fe_3O_4 greatly affects the core-shell porosity [36, 37]. The thicker the SiO_2 layer on the surface of the core Fe_3O_4 NP, the greater the porous volume. In addition, the presence of Fe_3O_4 NPs that are larger than SiO_2 (3:1) also affects the decrease in the porous volume of the core-shell material because of thinning of the shell thickness.

Table 2 The porosity of the Fe_3O_4/SiO_2 core-shell

Samples (Fe_3O_4:SiO_2)	Pore diameter (Å)		Surface area (m^2/g)		Pore volume (cm^3/g)	
	BET	BJH	BET	BJH	BET	BJH
1:1	88.07	17.30	204	80.46	0.893	0.971
1:3	45.64	8.45	3.56	25.98	0.165	0.177
3:1	2.78	12.97	3.37	12.11	0.035	0.052

Figure 12 also shows the isotherm nitrogen gas adsorption-desorption curves of the Fe_3O_4/SiO_2 core-shell to the relative pressure (P/Po) that also showed the porous volume space of the Fe_3O_4/SiO_2 particles with the adsorption and absorption processes. Furthermore, the curves can be used to determine the porous surface area using BET Equation (1) [37, 38]. The BET Equation (1) can be extrapolated from the linear data located at a relative pressure between 0.1 and 0.35 on the adsorption-desorption curve. The basic BET equation can determine the pore surface area [37-39]. With the provision of molecular weight and the cross-section of nitrogen being 28.013 gm and 16.2 A°, respectively, the data can be used to obtain the pore diameter and pore volume. In addition, supporting data can also be calculated using the BJH and DH methods [37-39]; the results are presented in Table 2.

$$\frac{1}{W\left[\left(\frac{P_0}{P}\right)-1\right]}=\frac{1}{W_m C}+\left[\frac{C-1}{W_m C}\right]\frac{P}{P_0} \quad (1)$$

W is the weight of the absorbed gas (adsorbate) at the relative pressure P/P_0; *Wm* is the weight of the gas (adsorbate) that forms the monolayer on the surface of the solid; P is the adsorption equilibrium pressure; P_0 is the saturation pressure from the sample adsorption at the cooling bath temperature, P/P_0 denotes the relative pressure of adsorption, and C is the energy constant. Equations (2) and (3) were used to calculate the total surface area and SSA [37, 38].

$$S_{total}=\frac{W_m N_a A_{cs}}{V} \quad (2)$$

$$S_p=\frac{S_{total}}{M} \quad (3)$$

S_{total} is the total surface area (m^2/gr), S_p is a SSA (m^2/g), *Na* is Avogadro's number (6.02×10^{23} molecule/mol), M is the weight of the nitrogen gas (*g*), A_{cs} is the BET constant, and V denotes the trailer molar volume.

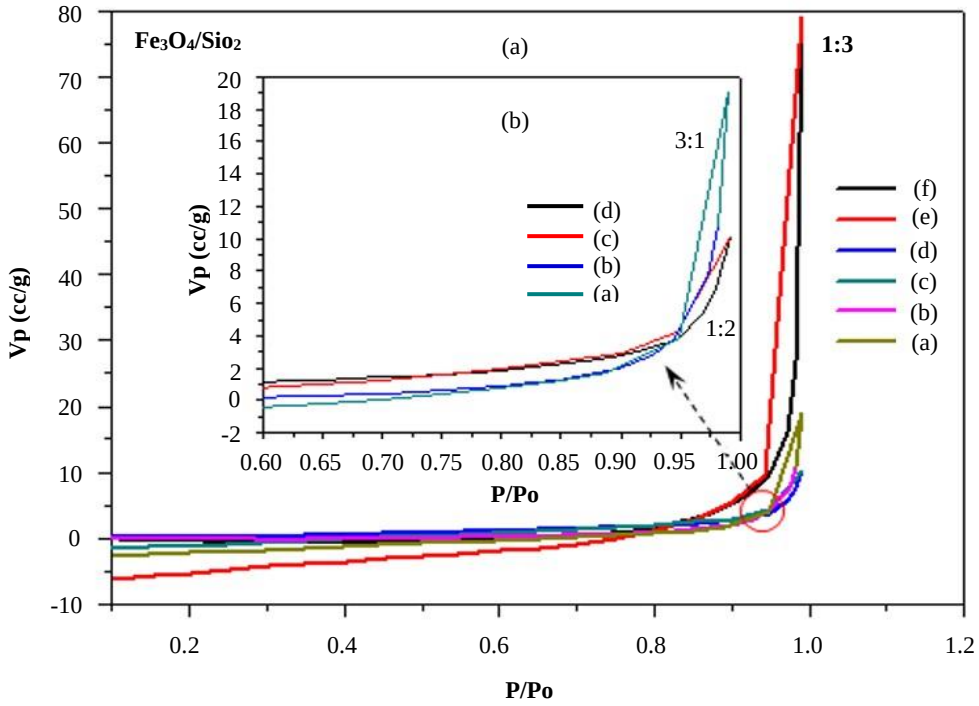

Figure 12 Nitrogen gas adsorption-desorption curves for Fe_3O_4/SiO_2 core-shell samples with (a) 1:2, 1:3, and 3:1 compositions. The insert is a magnification of the (b) 1:2 and 3:1 composition.

The shape of the hysteresis curve (Figure 12) indicates an H_3 curve with type B sorption gas, with porous particle formation slits [11]. The pore diameter, surface area, and pore volume because of the three analysis methods (BET, BJH, and DH) are shown in Table 2. The pore volume decreased with an increase in the mass fraction of SiO_2 NPs. The BET analysis results of the 1:2 sample had a pore diameter of~88.07 A°, the pore volume was~0.892 cc/g, and the surface of the pore area was~204 m^2/g. The 1:2 sample had higher pore diameter, surface area, and pore volume values than the 1:3 and 3:1 samples. Based on the BET theory, a large surface area depends on a relatively small pore size [33, 36, 37].

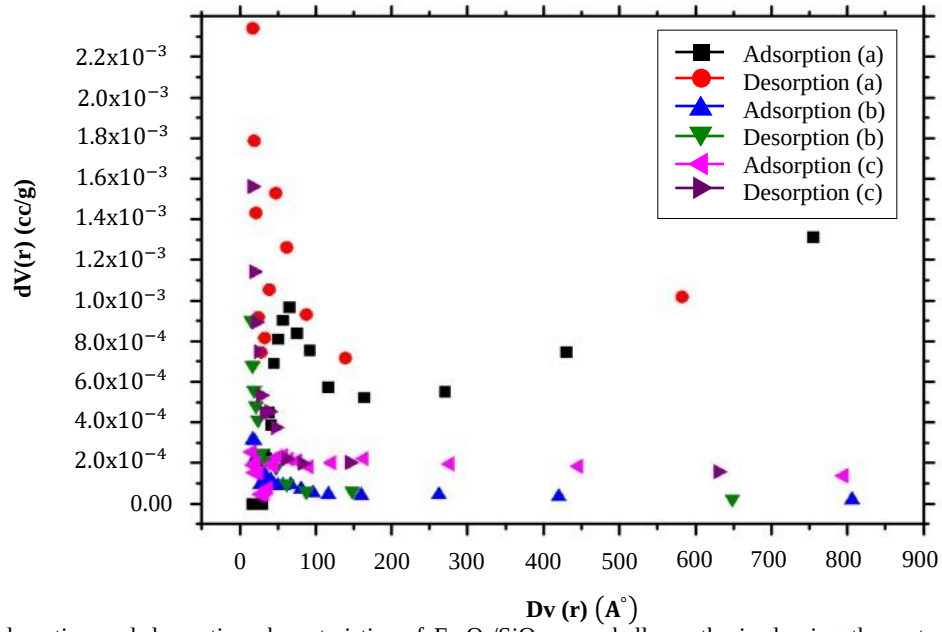

Figure 13 Adsorption and desorption characteristics of Fe_3O_4/SiO_2 core-shells synthesized using the wet mixing method with a Fe_3O_4:SiO_2 mass ratio of (a) 1:2, (b) 1:3, and (c) 3:1.

Figure 13 shows the pore diameter distribution Dv (r) to dV (r) on the Fe_3O_4/SiO_2 nanocomposite in the adsorption and desorption processes of nitrogen gas using the BET method. The 1:2 sample has a pore diameter between 3.44 and 150.80 nm, Sample #2 has a pore diameter between 3.09 and 3.38 nm, and the 3:1 sample has a pore diameter between 3.05 and 3.41. There appears to be a wide enough range for the 1:2 sample, which indicates dV (r) with Dv (r) shows a more significant pattern. The difference in pore size can occur because of the large number of silanol groups (≡Si-OH), which can affect the pore size distribution. However, the pore diameter also depends on the pore structure formed [39-41]. The increased mass fraction of the SiO_2 NPs in the Fe_3O/SiO_2 material will reduce the porosity size. This is evident in Figures 12 and 13; the trend of the P/P_0 hysteresis curve toward pore volume and $D_v(r)$ against dV(r) decreases for the 1:2, 1:3, and 3:1 samples, respectively.

4.4 Methylene-blue degradation of Fe_3O_4/SiO_2 core-shell nanoparticles

Methylene blue (MB) is a cationic colorant that can cause several harmful effects. Acute exposure to MB can cause increased heart rate, vomiting, shock, cyanosis, and tissue necrosis in humans. In the process of treating industrial waste, such as textile industries, any paper that has a lot of colored synthetic or organic chemicals should also be treated before disposal; otherwise, the dye will enter the soil and the water will be consumed by humans [36, 37].

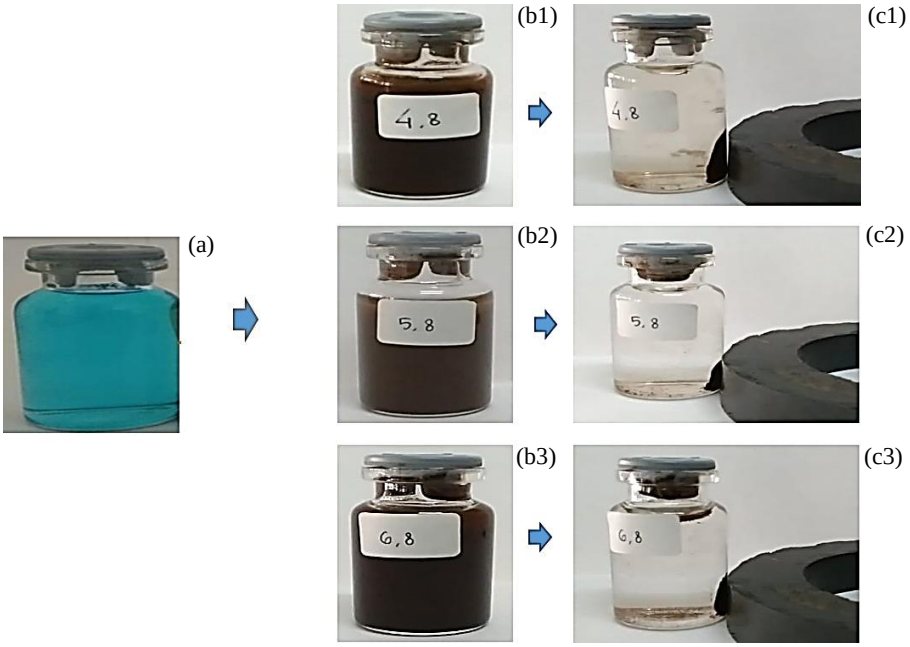

Figure 14 Examples of the absorption of methylene-blue dye by Fe_3O_4/SiO_2 adsorbent prepared using the in-situ method (for TEOS volumes of 4.8, 5.8, and 6.8 mL): (a) water with methylene-blue dye, (b) after the addition of adsorbent, and (c) absorption of methylene blue by Fe_3O_4/SiO_2 adsorbent.

Rapid detection and removal of dyes from contaminated water is a prevalent problem for the environment and human existence because of its high toxicity, chemical stability, and low degradability. Based on the experiments, the Fe_3O_4/SiO_2 samples that have the basic properties of superparamagnetic Fe_3O_4 can detect MB quickly and eliminate dyes in water [7, 39, 40], while under an external magnetic field (as illustrated in Figure 14). Rapid redox reactions of Fe(+3) and Fe(+2) can be achieved (31), and composite catalysts (Fe_3O_4/SiO_2) have great potential for breaking down organic compounds. Several previous studies indicated the use of graphene (GO) as a wrapper for Fe_3O_4 and decorating TiO_2 (Fe_3O_4@GO-TiO_2) for photocatalyst applications [10, 42]. Quantitative analysis can use the same method as previous studies [9, 37], which calculates the removal percentage and amount of dye adsorbed by the adsorbent under equilibrium conditions.

Figure 14 illustrates the MB adsorption process with core-shell samples of Fe_3O_4/SiO_2 with variations in the composition of TEOS volume [26, 33, 42]. As shown in Figures 14(a) and 14(b1-b3), a bottle containing MB solution was incorporated with Fe_3O_4/SiO_2 powder and it appeared black. The solution was then shaken and allowed to settle (5-10 min). The dye from the MB solution changed color to nano-spare black. The next step is to place an external magnet, as shown in Figures 14(c1-c3). The pure water and MB absorbed by Fe_3O_4/SiO_2 particles will separate in the external magnetic field (there is sediment). The adsorption for each sample prepared with different volume variations of TEOS (in situ process) was the same. The deposition rate or adsorption rate was faster for lesser TEOS compositions (6.8 ml), which is consistent with the greater maximum ability of magnetization (M). Figure 15 illustrates the UV-Vis spectroscopy of MB. After adding Fe_3O_4/SiO_2 core-shell to the MB solution, the dominant dye color from MB was absorbed by the Fe_3O_4/SiO_2 core-shell with mass variation. The adsorption intensity (λ_m) of MB is 2.8937; each adsorbate mass of Fe_3O_4/SiO_2: 0.07 gm, 0.14 gm, and 0.21 gm (Figure 15) indicates an adsorption intensity of 2.134, 1.173, and 0.6747, respectively.

The intensity of the UV-Vis graph for samples with varying concentrations of adsorbate (MB): 10-60 ppm (10, 20, 30, 40, 50, and 60 ppm), each showing adsorption intensities of 0.0518, 0.0936, 0.1369, 0.2325, 0.5228, and 0.8934, respectively (Figure 16). Figure 16 illustrates the adsorption rate of adsorbent (Fe_3O_4/SiO_2 powder) against MB with varying concentrations, from 10 to 50 ppm. The higher the adsorbate concentration, the less dye absorbed by the adsorbent because the adsorption capacity or the pore adsorbent particles were filled by the absorbed substance particles dyes. This is graphically marked by the higher the transmittance intensity of the UV-Vis spectroscopy, along with the increase in ppm of the test solution. In addition, there will be an increasing trend of dye absorbed by the adsorbate if the length of time spent in the adsorption process is longer (Figure 17). This is indicated graphically; by increasing the duration of time 2.5-30 min, the intensity of the transmittance decreases, as shown in Figure 17. At 2.5 min, the absorbance intensity was~0.2332. Within 30 min, it was~0.0803. This decrease in evidence time also affects the dye adsorption process by a core-shell adsorbent.

Based on the UV-Vis spectroscopy data for variations in the adsorbent mass, adsorbate (distilled water with MB dye) and duration of adsorption time as presented in Figures 15-17; the dyes-removal efficiency (DRE_{MB}) of the Fe_3O_4/SiO_2 core-shell for the sample (6.8 mL) can be estimated as shown Figure 18 [26, 42]. DRE_{MB} will increase as the time duration and mass of the adsorbent increase. The higher the absorption capacity of the core-shell in absorbing the MB dye, the more limited the concentration. At a certain point, the absorption capacity will experience a saturation phase. As shown in Figure 18, for a time duration of 2.5 min, the DR_{EMB} was 66.73% and at 30 min it was 88.54%. The same trend for the 0.07 gm core-shell mass provided an efficiency of 26.25%, and for 0.21 gram, the DRE_{MB} was 76.68% (an increase occurs).

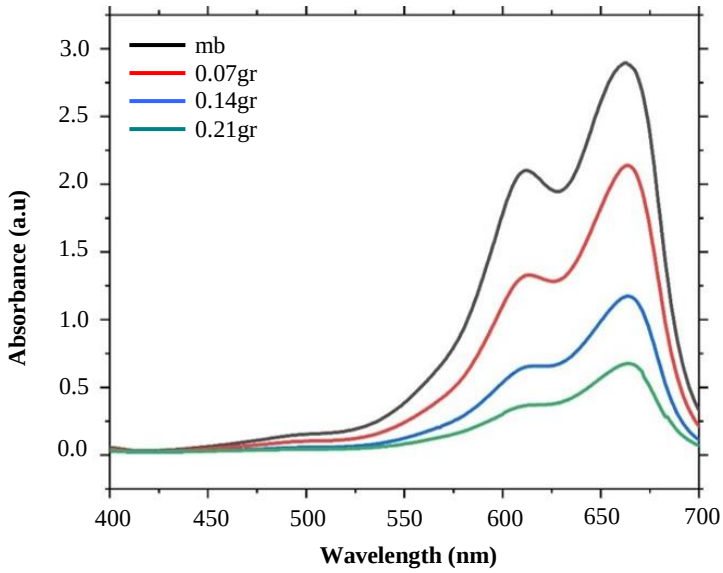

Figure 15 UV-Vis Spectroscopy of water absorptivity with MB by adsorbent (Fe_3O_4/SiO_2 core-shells (6.8 mL TEOS)): 0.07, 0.14, and 0.21 g.

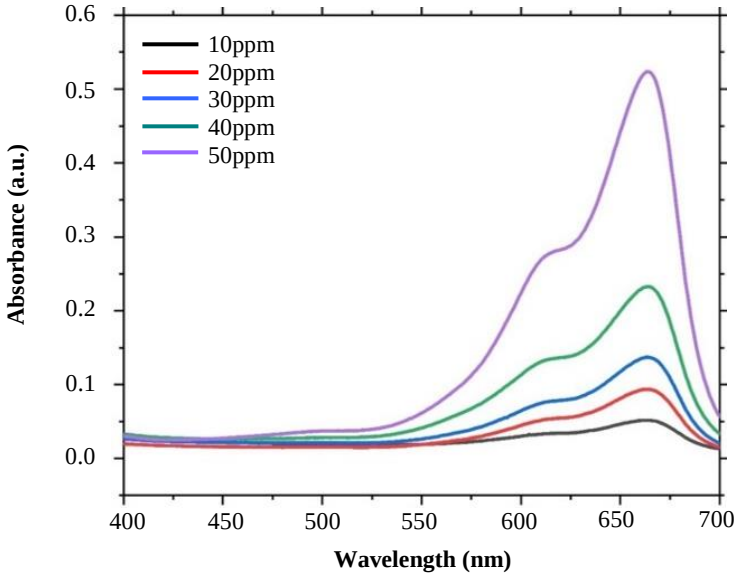

Figure 16 UV-Vis Spectroscopy of 10, 20, 30, 40, and 50 ppm methylene blue (MB) by 0.21 grams of adsorbent.

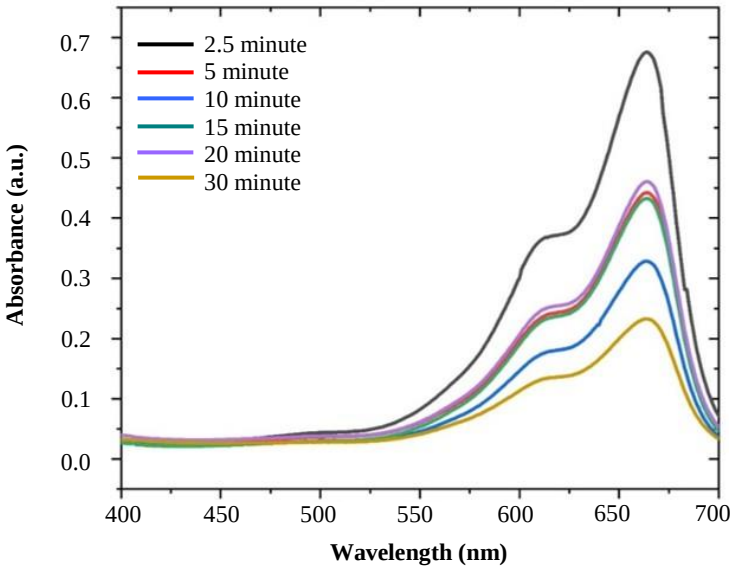

Figure 17 UV-Vis Spectroscopy of MB solution by Fe_3O_4/SiO_2 core-shell (6.8 mL TEOS) adsorbate over 2.5, 5, 10, 15, 20, and 30 min.

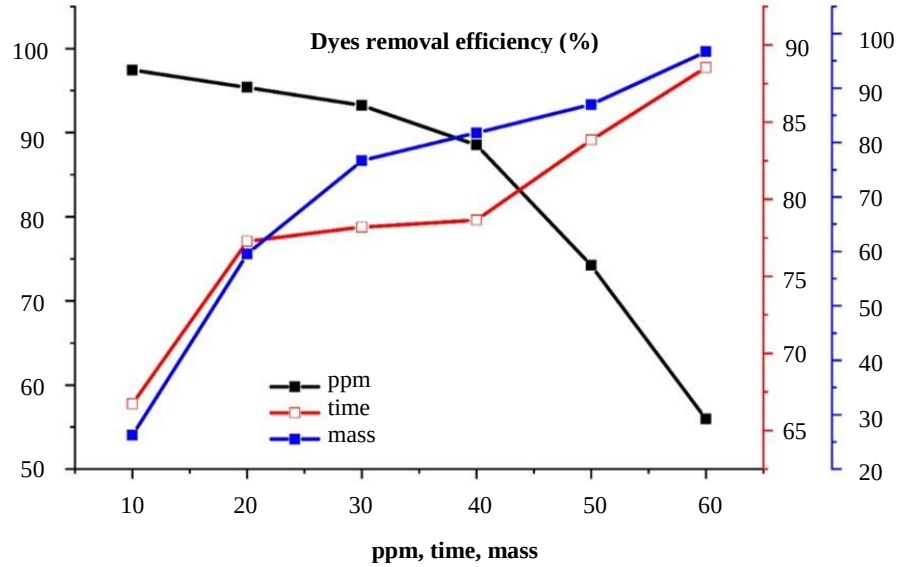

Figure 18 Dye-removal efficiency (DRE_{MB}) by Fe_3O_4/SiO_2 core-shell (6.8 mL TEOS) as adsorbent with mass variation, concentration (ppm) of adsorbate, and time duration of adsorption.

5. Conclusions

Fe_3O_4 NPs were successfully synthesized from iron sand minerals extracted by the co-precipitation method, and the SiO_2 (amorphous) NPs were extracted from silica sand. The synthesis of Fe_3O_4/SiO_2 core-shell NPs was successfully conducted using two methods: (i) wet mixing method and (ii) in situ method. The crystalline structure of the core-shell is in the magnetite phase with a functional group of Fe-O-Fe and Si-O-Si bonds, which are indicators of the surface coating of Fe_3O_4 NPs by SiO_2 particles. The morphological analysis shows a single core-shell with NP size (below 50 nm) and a shell (~10 nm). The magnetic properties of the Fe_3O_4 NPs were controlled by increasing the content of SiO_2 particles in the Fe_3O_4/SiO_2 composites. Magnetic property analysis showed that increasing the SiO_2 shell and PEG content significantly reduced the magnetization strength of the Fe_3O_4 NPs (32.9%-67.8%). The magnetization curve reinforced the argument that the Fe_3O_4/SiO_2 composite NPs constructed a superparamagnetic material. Furthermore, this material exhibited excellent adsorption properties for dye solutions such as methylene blue.

6. Acknowledgments

This research was supported by Universitas Negeri Surabaya (UNESA). The researcher (M) also expresses his gratitude to RISTEK-BRIN, the Ministry of Education and Culture of the Republic of Indonesia and UNESA FMIPA Integrated Laboratory for their supports during the test and analysis of samples.

7. References

[1] Todini E. Paradigmatic changes required in water resources management to benefit from probabilistic forecasts. Water Secur. 2018;3:9-17.
[2] Petrie B, Barden R, Kasprzyk-Hordern B. A review on emerging contaminants in wastewaters and the environment: current knowledge, understudied areas and recommendations for future monitoring. Water Res. 2015;72:3-27.
[3] Gupta N, Pandey P, Hussain J. Effect of physicochemical and biological parameters on the quality of river water of Narmada, Madhya Pradesh, India. Water Sci. 2017;31(1):11-23.
[4] Dewanto AS, Kusumawati DH, Putri NP, Yulianingsih A, Sa'adah IKF, Taufiq A, et al. Structure analysis of Fe_3O_4@SiO_2 core shells prepared from amorphous and crystalline SiO_2 particles. IOP Conf Ser Mater Sci Eng. 2018;367:012010.
[5] Tamez C, Hernandez R, Parsons JG. Removal of Cu (II) and Pb (II) from aqueous solution using engineered iron oxide nanoparticles. Microchem J. 2016;125:97-104.
[6] Hou S, Li X, Wang H, Wang M, Zhang Y, Chi Y, et al. Synthesis of core–shell structured magnetic mesoporous silica microspheres with accessible carboxyl functionalized surfaces and radially oriented large mesopores as adsorbents for the removal of heavy metal ions. RSC Adv. 2017;7(82):51993-2000.
[7] Yang L, Tian J, Meng J, Zhao R, Li C, Ma J, et al. Modification and characterization of Fe_3O_4 nanoparticles for use in adsorption of alkaloids. Molecules. 2018;23(3):562.
[8] Carlos L, Garcia Einschlag FS, González MC, Mártire DO. Applications of magnetite nanoparticles for heavy metal removal from wastewater. In: Garca Einschlag FS, editor. WasteWater - Treatment Technologies and Recent Analytical Developments. London: InTech; 2013. p. 63-77.
[9] Konate A, He X, Zhang Z, Ma Y, Zhang P, Alugongo GM, et al. Magnetic (Fe_3O_4) nanoparticles reduce heavy metals uptake and mitigate their toxicity in wheat seedling. Sustainability. 2017;9(5):790.
[10] Yang S, Zeng T, Li Y, Liu J, Chen Q, Zhou J, et al. Preparation of graphene oxide decorated Fe_3O_4@SiO_2 nanocomposites with superior adsorption capacity and SERS detection for organic dyes. J Nanomater. 2015;2015:817924.
[11] Kakavandi B, Jonidi A, Rezaei R, Nasseri S, Ameri A, Esrafily A. Synthesis and properties of Fe_3O_4-activated carbon magnetic nanoparticles for removal of aniline from aqueous solution: equilibrium, kinetic and thermodynamic studies. Iranian J Environ Health Sci Eng. 2013;10:19.

[12] Peng X, Wang Y, Tang X, Liu W. Functionalized magnetic core–shell Fe_3O_4@SiO_2 nanoparticles as selectivity-enhanced chemosensor for Hg (II). Dye Pigment. 2011;91(1):26-32.
[13] Ding HL, Zhang YX, Wang S, Xu JM, Xu SC, Li GH. Fe_3O_4@ SiO_2 core/shell nanoparticles: the silica coating regulations with a single core for different core sizes and shell thicknesses. Chem Mater. 2012;24(23):4572-80.
[14] Hui C, Shen C, Tian J, Bao L, Ding H, Li C, et al. Core-shell Fe_3O_4@SiO_2 nanoparticles synthesized with well-dispersed hydrophilic Fe 3 O 4 seeds. Nanoscale. 2011;3(2):701-5.
[15] Pasandideh EK, Kakavandi B, Nasseri S, Mahvi AH, Nabizadeh R, Esrafili A, et al. Silica-coated magnetite nanoparticles core-shell spheres (Fe_3O_4@SiO_2) for natural organic matter removal. J Environ Heal Sci Eng. 2016;14:1-13.
[16] Lai L, Xie Q, Chi L, Gu W, Wu D. Adsorption of phosphate from water by easily separable Fe_3O_4@SiO_2 core/shell magnetic nanoparticles functionalized with hydrous lanthanum oxide. J Colloid Interface Sci. 2016;465:76-82.
[17] Emadi M, Shams E, Amini MK. Removal of zinc from aqueous solutions by magnetite silica core-shell nanoparticles. J Chem. 2013;2013:787682.
[18] Beg MS, Mohapatra J, Pradhan L, Patkar D, Bahadur D. Porous Fe_3O_4-SiO_2 core-shell nanorods as high-performance MRI contrast agent and drug delivery vehicle. J Magn Magn Mater. 2017;428:340-7.
[19] Farimani MHR, Shahtahmasebi N, Roknabadi MR, Ghows N, Kazemi A. Study of structural and magnetic properties of superparamagnetic Fe_3O_4/SiO_2 core–shell nanocomposites synthesized with hydrophilic citrate-modified Fe_3O_4 seeds via a sol–gel approach. Phys E Low-dimensional Syst Nanostructures. 2013;53:207-16.
[20] Ghazanfari MR, Kashefi M, Shams SF, Jaafari MR. Perspective of Fe_3O_4 nanoparticles role in biomedical applications. Biochem Res Int. 2016;2016:7840161.
[21] Zhang L, Shao H, Zheng H, Lin T, Guo Z. Synthesis and characterization of Fe_3O_4@SiO_2 magnetic composite nanoparticles by a one-pot process. Int J Miner Metall Mater. 2016;23(9):1112-8.
[22] Rahmawati R, Taufiq A, Sunaryono S, Fuad A, Yuliarto B, Suyatman S, et al. Synthesis of magnetite (Fe_3O_4) nanoparticles from iron sands by coprecipitation-ultrasonic irradiation methods. J Mater Environ Sci. 2018;9(3):155-60.
[23] Khatami M, Alijani HQ, Nejad MS, Varma RS. Core@ shell nanoparticles: greener synthesis using natural plant products. Appl Sci. 2018;8(3):411.
[24] Supardi ZAI, Nisa Z, Kusumawati DH, Putri NP, Taufiq A, Hidayat N. Phase transition of SiO_2 nanoparticles prepared from natural sand: the calcination temperature effect. J Phys Conf Ser. 2018;1093:012025.
[25] Jal PK, Sudarshan M, Saha A, Patel S, Mishra BK. Synthesis and characterization of nanosilica prepared by precipitation method. Colloids Surfaces A Physicochem Eng Asp. 2004;240(1-3):173-8.
[26] Munasir N, Kusumawati RP, Kusumawati DH, Supardi ZAI, Taufiq A, Darminto D. Characterization of Fe_3O_4/rGO composites from natural sources: application for dyes color degradation in aqueous solution. Int J Eng. 2020;33(1):18-27.
[27] Terraningtyas A. Synthesis and characterization of Fe_3O_4/SiO_2 composite with in-situ method: TEOS as SiO_2 NPs precursor. J Phys Conf Ser. 2019;1171:012050.
[28] Dewanto AS, Yulianingsih A, Saadah IKF, Supardi ZAI, Mufid A, Taufiq A. Composites of Fe_3O_4@SiO_2 from natural material synthesized by co-precipitation method. IOP Conf Ser Mater Sci Eng. 2017;202:012057.
[29] Deng H, Lei Z. Preparation and characterization of hollow Fe_3O_4/SiO_2@ PEG–PLA nanoparticles for drug delivery. Compos Part B Eng. 2013;54:194-9.
[30] Zhang X, Huang Z, Ma B, Wen R, Zhang M, Huang Y, et al. Polyethylene glycol/Cu/SiO 2 form stable composite phase change materials: preparation, characterization, and thermal conductivity enhancement. RSC Adv. 2016;6(63):58740-8.
[31] Byrne JM, Klueglein N, Pearce C, Rosso KM, Appel E, Kappler A. Redox cycling of Fe (II) and Fe (III) in magnetite by Fe-metabolizing bacteria. Science. 2015;347(6229):1473-6.
[32] Drissi SH, Refait P, Abdelmoula M, Génin J-MR. The preparation and thermodynamic properties of Fe (II)/Fe (III) hydroxide-carbonate (green rust 1); Pourbaix diagram of iron in carbonate-containing aqueous media. Corros Sci. 1995;37(12):2025-41.
[33] Nikmah A, Taufiq A, Hidayat A. Synthesis and characterization of Fe_3O_4/SiO_2 nanocomposites. IOP Conf Ser Earth Environ Sci. 2019;276:012046.
[34] Taib S, Suharyadi E. Sintesis Nanopartikel Magnetit (Fe_3O_4) Dengan Template Silika (SiO_2) dan Karakterisasi Sifat Kemagnetannya. Indones J Appl Phys. 2015;5(1):23-30. (In Indonesia)
[35] Morrow BA, McFarlan AJ. Surface vibrational modes of silanol groups on silica. J Phys Chem. 1992;96(3):1395-400.
[36] Quercia G, Lazaro A, Geus JW, Brouwers HJH. Characterization of morphology and texture of several amorphous nano-silica particles used in concrete. Cem Concr Compos. 2013;44:77-92.
[37] Sun S, Liang F, Tang L, Wu J, Ma C. Microstructural investigation of gas shale in Longmaxi formation, Lower Silurian, NE Sichuan basin, China. Energy Explor Exploit. 2017;35(4):406-29.
[38] Trunschke A. Modern Methods in Heterogeneous Catalysis Research: Surface area and pore size determination [Internet]. 2017 [cited 2021 Nov 01]. Available form: http://www.fhi-berlin.mpg.de/acnew/department/pages/teaching/pages/teaching__winter semester__2017_2018/annette_trunschke__surface_area_and_pore_size_determination__171124.pdf.
[39] Ubaid A, Hidayat N. Aging time effect on porous characteristics of natural mud-based silica prepared by hydrothermal-coprecipitation route. IOP Conf Ser Mater Sci Eng. 2017;202:012022.
[40] Zhu M, Diao G. Synthesis of porous Fe_3O_4 nanospheres and its application for the catalytic degradation of xylenol orange. J Phys Chem C. 2011;115(39):18923-34.
[41] Pirbazari AE, Saberikhah E, Kozani SSH. Fe_3O_4–wheat straw: preparation, characterization and its application for methylene blue adsorption. Water Resour Ind. 2014;7:23-37.
[42] Tian Q, Wang X, Mao F, Guo X. Absorption performance of DMSA modified Fe_3O_4@SiO_2 core/shell magnetic nanocomposite for Pb 2+ removal. J Cent South Univ. 2018;25(4):709-18.